ISSN 0016-7029, Geochemistry International, 2006, Vol. 44, No. 2, pp. 118–136. © Pleiades Publishing, Inc., 2006.
Original Russian Text © V.A. Kovalenker, V.B. Naumov, V.Yu. Prokof'ev, S. Jelen, M. Gaber, 2006, published in Geokhimiya, 2006, No. 2, pp. 141–160.

Compositions of Magmatic Melts and Evolution of Mineral-Forming Fluids in the Banska Stiavnica Epithermal Au–Ag–Pb–Zn Deposit, Slovakia: A Study of Inclusions in Minerals

V. A. Kovalenker*, V. B. Naumov, V. Yu. Prokof'ev*, S. Jelen***, and M. Gaber*****

**Institute of Geology of Ore Deposits, Petrography, Mineralogy, and Geochemistry (IGEM), Russian Academy of Sciences, Staromonetnyi per. 35, Moscow, 109017 Russia*

e-mail: kva@igem.ru

***Vernadsky Institute of Geochemistry and Analytical Chemistry, Russian Academy of Sciences, ul. Kosygina 19, Moscow, 119991 Russia*

e-mail: naumov@geokhi.ru

****Geological Institute, Academy of Sciences of Slovakia, Banska Bystrica Department, Severna 5, Banska Bystrica, 97401 Slovakia*

e-mail: jelen@savbb.sk

Received July 1, 2004

Abstract—Melt and fluid inclusions were investigated in minerals from igneous rocks and ore (Au–Ag–Pb–Zn) veins of the Stiavnica ore field in Central Slovakia. High H_2O (7.1–12.0 wt %) and Cl (0.32–0.46 wt %) contents were found in silicate melt inclusions (65–69 wt % SiO_2 and 5.2–5.6 wt % K_2O) in plagioclase phenocrysts (*An* 68–36) from biotite–hornblende andesites of the eastern part of the caldera. Similar high water contents are characteristic of magmatic melts (71–76 wt % SiO_2 and 3.7–5.1 wt % K_2O) forming the sanidine rhyolites of the Vyhne extrusive dome in the northwestern part of the Stiavnica caldera (up to 7.1 wt %) and the rhyolites of the Klotilda dike in the eastern part of the ore field (up to 11.5 wt %). The examination of primary inclusions in quartz and sanidine from the Vyhne rhyolites revealed high concentrations of N_2 and CO_2 in magmatic fluid (8.6 g/kg H_2O and 59 g/kg H_2O, respectively). Fluid pressure was estimated as 5.0 kbar on the basis of primary CO_2 fluid inclusions in plagioclase phenocrysts from the Kalvari basanites. This value corresponds to a depth of 18 km and may be indicative of a deep CO_2 source. Quartz from the granodiorites of the central part of the Stiavnica–Hodrusa complex crystallized from a melt with 4.2–6.1 wt % H_2O and 0.24–0.80 wt % Cl. Magmatic fluid cogenetic with this silicate melt was represented by a chloride brine with a salinity of no less than 77–80 wt % NaCl equiv. Secondary inclusions in quartz of the igneous rocks recorded a continuous trend of temperature, pressure, and solution salinity, from the parameters of magmatic fluids to the conditions of formation of ore veins. The gold mineralization of the Svyatozar vein system was formed from boiling low-salinity fluids (0.3–8.0 wt % NaCl equv.) at temperatures of 365–160°C and pressures of 160–60 bar. The Terezia, Bieber, Viliam, Spitaler, and Rozalia epithermal gold–silver–base metal veins were also formed from heterogeneous low-salinity fluids (0.3–12.1 wt %) at temperatures of 380–58°C and pressures of 240–10 bar. It was found that the salt components of the solutions were dominated by chlorides (high content of fluorine, up to 0.45 mol/kg H_2O, was also detected), and sulfate solutions appeared in the upper levels. The dissolved gas of ore-forming solutions was dominated by CO_2 (0.1–8.4 mol %, averaging 1.3 wt %) and contained minor nitrogen (0.00–0.85 mol %, averaging 0.05 mol %) and negligible methane admixtures (0.00–0.05 mol %, averaging 0.004 mol %). These data allowed us to conclude that the magmatic melts could be sources of H_2O, Cl, CO_2, and N_2. The formation of the epithermal mineralization of the Stiavnica ore field was associated with the mixing of magmatic fluid with low-concentration meteoric waters, and the fluid was in a heterogeneous state.

DOI: 10.1134/S0016702906020029

INTRODUCTION

There is increasing interest in the problems of formation of epithermal deposits owing to their continuously growing contribution to the inventory of the world's resources of noble and base metals, which has become especially clear during the past decades after the discovery and development of a number of large and giant deposits in island-arc and continental margin areas. Among the key problems arising during the investigation of these deposits are those related to the characterization of the fluid regime, including the estimation of physicochemical conditions, cation, anion,

and gas compositions of mineral-forming solutions, and proportions of magmatic and nonmagmatic components in them. Such data are of crucial importance for the evaluation of the transportation mechanisms of gold, silver, and other metals from the source to the deposition site and establishment of the main factors of their concentration as ore mineralization.

In the recent years, the use of modern analytical and isotope techniques and methods of inclusion investigation in studies of diverse epithermal mineralization in volcanic arcs of various regions and a comparison of the results of this work with the data on present-day geothermal and volcanic–hydrothermal systems have greatly improved our understanding of specific features of the development of ore-forming systems in volcanic structures and constrained their genetic models [e.g., 1–10]. However, one complex and not yet adequately solved problem is the detection of relationships between the evolution of a magma chamber, migration of magmatic fluids, changes in their physicochemical conditions and compositions, and formation of epithermal mineralization at the subsurface level of volcanic structures. Its solution is necessary for the further development and application of integrated genetic models of epithermal mineralization.

This paper focuses on the results of our study of melt and fluid inclusions in minerals from the igneous rocks and ore veins of the Banska Stiavnica epithermal Au–Ag–Pb–Zn deposit in Central Slovakia, which is one of the best known and thoroughly investigated deposits in Europe. This deposit has been mined since the time of the Roman Empire. According to archive data [11, 12], during the past 400 years, approximately 400 t Au, 6500 t Ag, 70 000 t Zn, 55 000 t Pb, and 8000 t Cu have been recovered in this deposit, which can be classified as a large one. It is a typical example of epithermal mineralization enriched in base-metal sulfides of the low-sulfidation [13] or sericite–adularia [14] type. In the recent years, the potential of epithermal noble-metal mineralization has been reassessed in the volcanic areas of the Mediterranean province and, in particular, in the neovolcanic zone of the western Carpathians. Comprehensive geological, petrological, mineralogical, geochemical, isotopic, fluid inclusion, and geochronological studies have been performed in this region [2, 11, 15–25], which provided a basis for a general genetic model of the ore-forming system of the Stiavnica stratovolcano.

In our opinion, the results of this study and their interpretation allowed us to track the evolution of physicochemical parameters and fluid composition from the moment of fluid release at the magmatic stage of evolution to the hydrothermal stage proper, and, therefore, significantly improved the model. Since the geologic structure and metallogenic development of the Stiavnica stratovolcano and related mineralization have been comprehensively discussed in numerous publications, this paper focuses on problems directly connected with the clarification of the evolution of parameters and compositions of mineral-forming solutions responsible for the formation of the epithermal vein mineralization.

OVERVIEW OF THE GEOLOGIC STRUCTURE, MAGMATISM, AND ORE MINERALIZATION OF THE STIAVNICA STRATOVOLCANO

The Banska Stiavnica deposit is confined to one of the largest volcanic areas in Europe, the Stiavnica andesite stratovolcano in the western part of the Central Slovakia neovolcanic region (Fig. 1). This region is located in the inner zone of the Carpathian arc, which is a major trans-European geologic structure of Mesozoic–Tertiary age. Volcanism appeared in this zone at the Late Neogene–Quaternary stage of development and was related to the subduction of the European plate beneath the Carpathian arc and back-arc spreading processes [11]. The structure of the prevolcanic Hercynian basement, which is made up of Late Paleozoic and Mesozoic sedimentary rocks in this zone, clearly indicates that this region is a structure of the Basin and Range type (horsts and grabens).

The Stiavnica andesite stratovolcano is 2500 km^2 in area. It comprises a large (18 × 22 km) caldera filled with andesite volcanics and a resurgent horst in the center exposing basement rocks and a large subvolcanic intrusive sequence, which is referred to as the Stiavnica–Hodrusa complex (Figs. 1, 2). The current model of the evolution of the stratovolcano and associated ore-forming system was constructed taking into account spatial and age relationships between the igneous rocks and various mineralization types, which were observed in the Stiavnica ore field [11]. This model distinguishes the precaldera, caldera, and postcaldera stages in the history of the stratovolcano.

The precaldera stage involved the formation of a large andesite stratovolcano and emplacement of some large sills and laccoliths of andesites and andesite porphyries in the base of the central part of the stratovolcano; denudation of the volcano, formation of a quartz-diorite intrusion in the northern part of the central zone, and development of an accompanying autonomous hydrothermal system, which produced extensive argillization-type alteration (quartz, pyrophyllite, and pyrite) and deposition of a small amount of base metal sulfides at great depths; the further denudation of the stratovolcano accompanied by the emplacement of a large bell-shaped pluton in the basement of the volcanic edifice, formation of magnetite skarns at the contact of granodiorites with carbonate rocks, and development of a local hydrothermal system above the central part of the granodiorite pluton, which produced veinlet and disseminated base-metal mineralization; and formation of stocks and a cluster of dikes of granodiorite and quartz diorite porphyry around the granodiorite pluton.

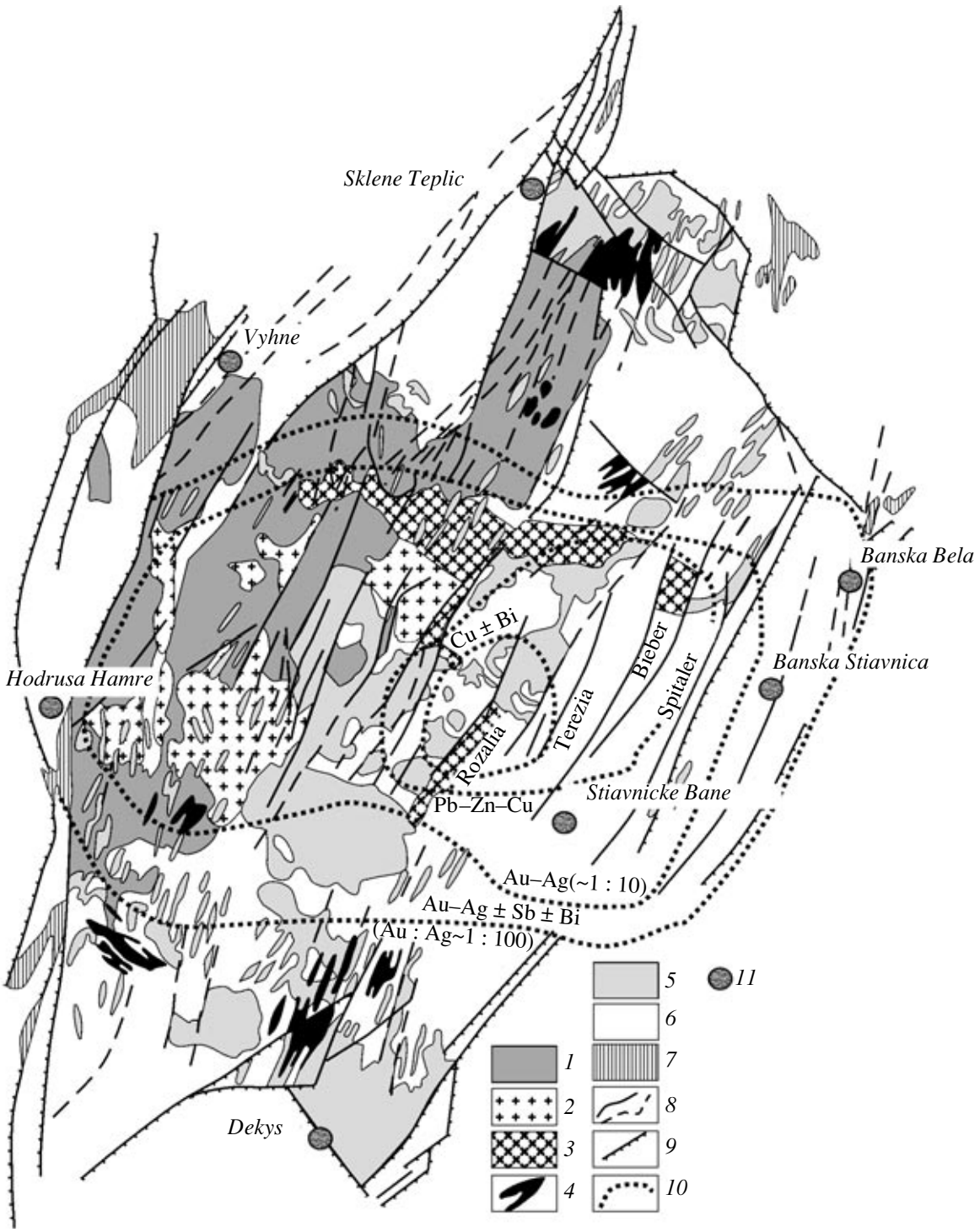

Fig. 1. Sketch map showing the structure and metallogeny of the Banska Stiavnica ore field, modified after [11]. (*1*) Pre-volcanic basement; (*2*) granodiorite; (*3*) diorite; (*4*) granodiorite porphyry; (*5*) sills and dikes of quartz diorite porphyry; (*6*) propylitized andesite and andesite porphyry; (*7*) rhyolite; (*8*) ore vein (solid line) and unmineralized fault (dashed line); (*9*) marginal fault of the resurgent horst; (*10*) boundary of mineral and geochemical zoning (names of zones are given on the map); and (*11*) major settlement. The names of major vein systems are given in normal font, and those of settlements are italicized.

The caldera stage involved caldera subsidence and filling with lacustrine sediments, redeposited tuffs, lavas and pyroclastic amphibole andesites and dacites (total thickness of up to 500 m), as well as emplacement of sills and ring dikes of quartz-diorite porphyries in a subvolcanic level.

During the postcaldera stage, eruptions of less evolved andesites resumed in individual centers at the

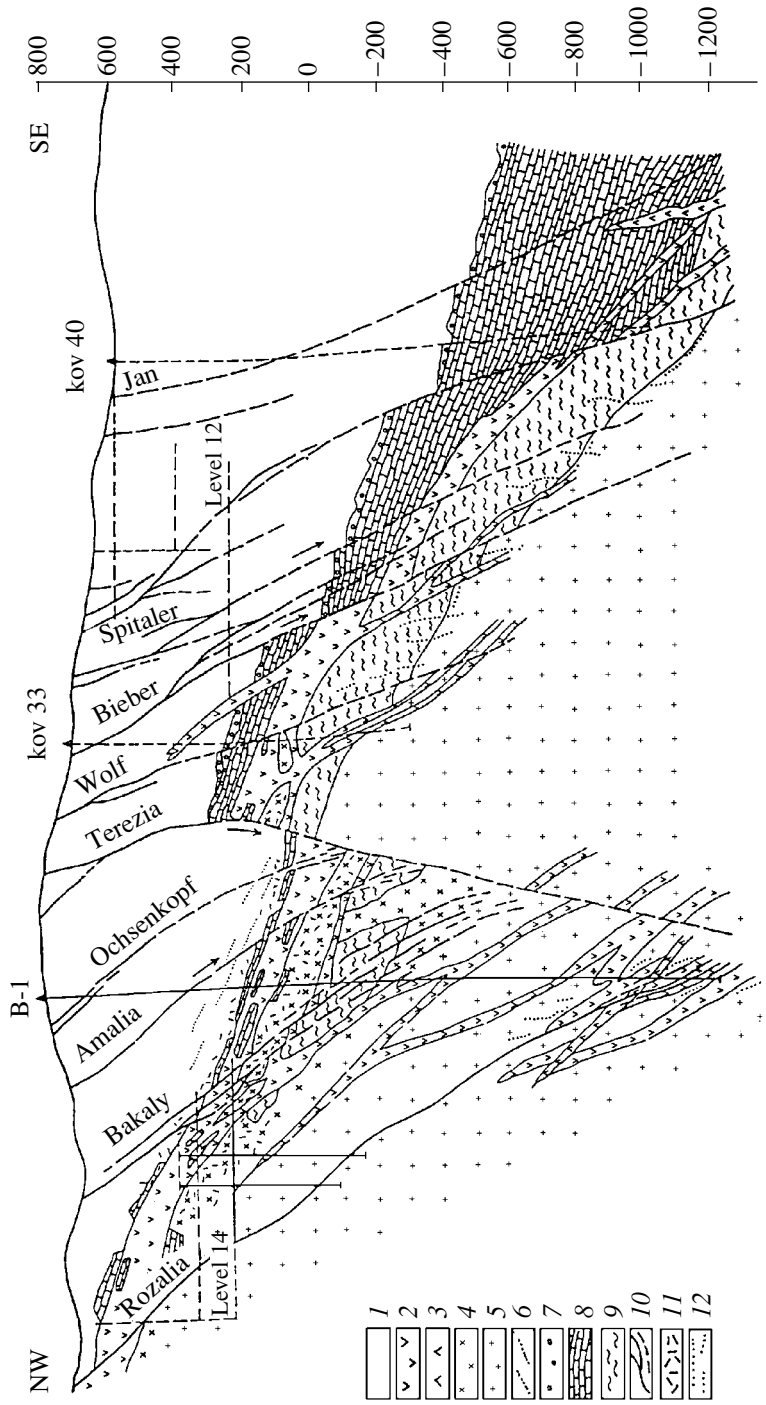

Fig. 2. Geological cross-section through the southwestern part of the Banska Stiavnica deposit [11]. (*1*) Precaldera andesite; (*2*) quartz–diorite porphyry; (*3*) granite porphyry (rhyolite); (*4*) granodiorite porphyry; (*5*) equigranular granodiorite; (*6*) thin aplite vein; (*7*) Paleogene conglomerate; (*8*) Triassic sedimentary rock; (*9*) schist; (*10*) postcaldera Au–Ag–base metal epithermal vein system; (*11*) veinlet–disseminated base metal mineralization; and (*12*) veinlets of Au–Ag–base metal mineralization. The B-1, kov 33, and kov 40 are boreholes.

slopes of the volcano and along the boundaries of the caldera, which coincided with the onset of horst upwelling and accompanied intrusion of rhyolites and granite porphyries in the zones of faults bounding the horst; appearance of a large epithermal system in the horst structure resulted in the formation of both base- and noble-metal sulfide-rich veins and gold–silver epithermal veins proper with a characteristic zoning and adularia–sericite alterations.

The volcanic rocks are chemically similar to medium- or high-potassium orogenic volcanic complexes of mature island arcs and continental margins, whereas the intrusive rocks of the Stianvnica–Hodrusa complex display a granodiorite trend, occasionally with a slight shift toward monzonites. Petrographic and geochemical investigations suggested a mantle source for the magmas with variable crustal contamination and differentiation in shallow magma chambers [19]. The origin of the late extrusive domes and dikes of rhyolites during the final stages of the development of the stratovolcano (exemplified by the Vyhne extrusive dome and Klotilda dike in our study) was related to melting of crustal material over a shallow magma chamber and magma mixing [19]. The youngest igneous rocks of the Stiavnica ore field are basaltoids, exemplified by the Kalvari and Kizigibel basanite necks, the formation of which was separated in time from the andesite stratovolcano proper by at least 3–4 Myr.

Several types of ore mineralization were distinguished in the central part of the caldera [18]: magnetite skarn, stockwork base-metal, metasomatic base-metal, lode Au–Ag, and epithermal Au–Ag–base metal. The ore mineralization is localized within or around the subvolcanic intrusive complex (Figs. 1, 2).

The epithermal Au–Ag and Au–Ag–base metal veins are of primary commercial importance. Overall, 120 vein systems are known within the deposit. They are from 2–3 to 7–9 km long, from 2–3 to 10–15 m thick, and from 200–300 to 700–1000 m in vertical extent [17, 19, 25]. Based on textural relationships, vertical extent, spatial distribution, and dominant mineral assemblages, Lexa *et al.* [18] distinguished three main types of epithermal veins, which are accompanied by the silicification, adularization, and sericitization of the subvolcanic and volcanic country rocks: (1) sulfide and base-metal rich epithermal veins of the Stiavnica type (e.g., the Bieber, Terezia, Rozalia, Spitaler, and other veins); (2) sulfide and base-metal poor silver-bearing epithermal veins of the Hodrusa type (Barenleuter, Mikulas, and other veins); and (3) gold–silver epithermal veins of the Kremnica type (Banska Bela, Kopanice, and Vyhne deposits). Since the ores of Hodrusa- and Kremnica-type veins had been extracted as early as the Middle Ages and are preserved only as museum samples, we will consider mainly the mineralization of the first (Stiavnica) type from the Terezia, Bieber, Spitaler, and Rozalia vein systems and gently sloping veins of the Svyatozar system.

The earliest and deepest among the Stiavnice-type vein systems studied are believed to be locally occurring gently sloping quartz-dominated epithermal Au–Ag (±Zn, Pb) veins of the Svyatozar system with banded and/or brecciated structures [18, 26]. They are located above the intrusive granodiorite massif and are roughly parallel to its roof. It was suggested [18] that at least the early phase of this mineralization is older than the quartz diorite porphyry sills that separate the granodiorites and blocks of mineralized andesites.

The majority of postcaldera vein systems with Stiavnica-type epithermal mineralization are confined to the faults of the Stiavnica–Hodrusa resurgent horst in the central part of the caldera over an area of about 100 km^2 (Fig. 1). The horst dips gently to the east and has an asymmetric structure. Most of the vein structures hosting epithermal mineralization are confined to the NNE–SSW trending faults in the eastern and southeastern parts of the horst and also dip to the east and southeast, except for the Terezia vein and several diagonal vein branches, which dip to the west (Fig. 2). The development of vein systems was controlled by the structural evolution of the horst, the uplift of which lasted for almost two million years, from the middle Sarmatian to the early Pannonian (approximately from 12.5 to 10.7 Ma) [16, 18]. The emplacement of extrusive domes and rhyolite dikes associating with the horst formation occurred mainly in the late stages of its evolution, mainly along marginal faults in the western and northwestern (uplifted mostly) parts of the horst (Fig. 1).

The distribution of epithermal mineralization exhibits a distinct mineralogical and geochemical zoning (Fig. 1): (a) the inner zone hosts base-metal veins with gold changing with depth into copper veins with bismuth in the eastern and central parts of the horst (Bieber and Rozalia vein systems); (b) the transitional zone hosts Au–Ag–base metal veins (Au : Ag ~ 1 : 100, Terezia and Spitaler vein systems); and (c) the outer zone hosts Au–Ag veins with subordinate amounts of base metals (Au : Ag ~ 1 : 10) confined to the horst-bounding faults. Similar changes of the types of mineralization were observed in the direction from the deep zone to the near-surface part of the deposit.

METHODS OF INVESTIGATION OF MELT AND FLUID INCLUSIONS IN MINERALS

Melt and fluid inclusions were investigated by various methods allowing determination of their compositions and formation conditions: optical examination, thermometric and cryometric experiments, gas and ion chromatography, ICP MS analysis of water extracts, and electron microprobe analysis.

Investigation of Inclusions of Magmatic Melt

Melt inclusions were homogenized by the quenching method using an electric furnace with a Pt heater [27] providing an accuracy of temperature control of ±10°C. The quenching method involves long (1–3 h) sample exposures under constant temperature, quenching of inclusions in air, and observation of the products of stepwise heating experiments at room temperature. The temperature increment between experiments decreased near phase transitions, which allowed us to determine with adequate accuracy both homogenization temperatures and the beginning of melting of silicate phases. It should be noted that silicate melt inclusions with high H_2O contents were extensively decrepitated upon heating above 500°C, and only small inclusions were occasionally homogenized. After quenching, the samples were polished to bring individual glass inclusions to the surface and analyzed on a Camebax Microbeam electron microprobe operating at 15 kV accelerating voltage and 30 nA beam current, rastering the beam over areas 12×12 or 5×5 μm. The accuracy of element measurement was 2% relative for element concentrations >10 wt %; 5% relative for concentrations of 5–10 wt %; and 10% relative for concentrations <5 wt %.

For inclusions of silicate melt with a visible aqueous liquid phase (i.e., for water-rich melts), the concentration of salts in the fluid was determined from the temperature of ice melting and volume proportions of phases, which allowed us to estimate the water content of the melt using the method of Naumov [28]. The maximum concentration of Cl in the melt was also estimated assuming that chlorides were the most abundant salts in the fluid.

Thermometric and Cryometric Investigations of Fluid Inclusions

The inclusions were explored using a set-up consisting of a THMSG-600 Linkam microscopic heating stage, an Amplival microscope equipped with a series of long-focus objectives, including a 80× Olympus objective, a video recorder, and a computer control system. The set-up allows us to perform real-time measurements of phase transition temperatures from –196 to +600°C, observe phase changes under high magnifications, and obtain digital photomicrographs. The concentrations of salts in the inclusions without dense gases were estimated from the melting temperature of ice using data from [29]. Pressure was determined for heterogeneous fluids using cogenetic inclusions homogenizing to both liquid and gas phases.

Gas Chromatography

The compositions of fluid inclusions were determined by chromatographic methods. Gas components and water were analyzed on a Tsvet 100M (model 163) gas chromatograph. The construction of the instrument and analytical methods were described by Mironova *et al.* [30]. The sensitivity of gas component determination was the following (μl): 1×10^{-2} N_2, 4×10^{-2} CH_4, 3×10^{-2} CO_2, and 5×10^{-5} H_2O.

Ion Chromatography

The anion composition of solutions was analyzed by ion chromatography [31], which provides several advantages over traditional methods in the range of analyzed anions (Cl^-, F^-, SO_4^{2-}, Br^-, $H_2PO_4^-$, NO_3^-, NO_2^-, anions of carbon acids, etc.), sample volume (0.01–0.1 ml), sensitivity (10^{-3} μg/ml), rapidity of analysis, high selectivity, and possibility of simultaneous measurement of inorganic and organic ions. Before analysis, monomineralic quartz, sphalerite, carbonates, and barite samples (grain size of 0.8–0.5 mm and weight of 0.3–0.6 g) were repeatedly washed with hot distilled water (quartz samples, with diluted hot HNO_3) and dried at a temperature of about 80°C. Inclusions were opened by the thermal method. The decrepitated sample was mixed in the same quartz insert with twice-distilled water in the proportion 1 : 1 and stirred for about 10 min to ensure complete dissolution of salt components ejected from inclusions during decrepitation. The extract was decanted and its anion composition was analyzed by ion chromatography. The concentrations of anions in the solution were calculated using the water content determined in the same charge, which improved the reliability of estimates.

Analysis of Water Extracts by ICP MS

The analysis of water extracts from inclusions by the method of inductively coupled plasma mass spectrometry is a complex multistage process. A monomineralic fraction with a grain size of 1.0–0.5 mm was separated from a sample in which fluid inclusions were preliminarily explored and the predominance of a certain inclusion type was established. The temperature of decrepitation of the majority of inclusions was initially determined in the mineral separate using a vacuum furnace. The amount of water in the inclusions was then determined using a gas chromatograph. A background solution and an extract proper were prepared from a 500-mg aliquot of the prewashed and dried monomineralic fraction. The background solution was prepared before the opening of vacuoles, after which the thermal decrepitation of inclusions was performed (usually at a temperature of 450°C) and sample solution was prepared. The volumes of the sample and background solutions were equal (dilution of 1 : 10). The contents of elements were calculated as a difference between the concentrations and recalculated to the mass of solution of inclusions using the amount of water determined by gas chromatography.

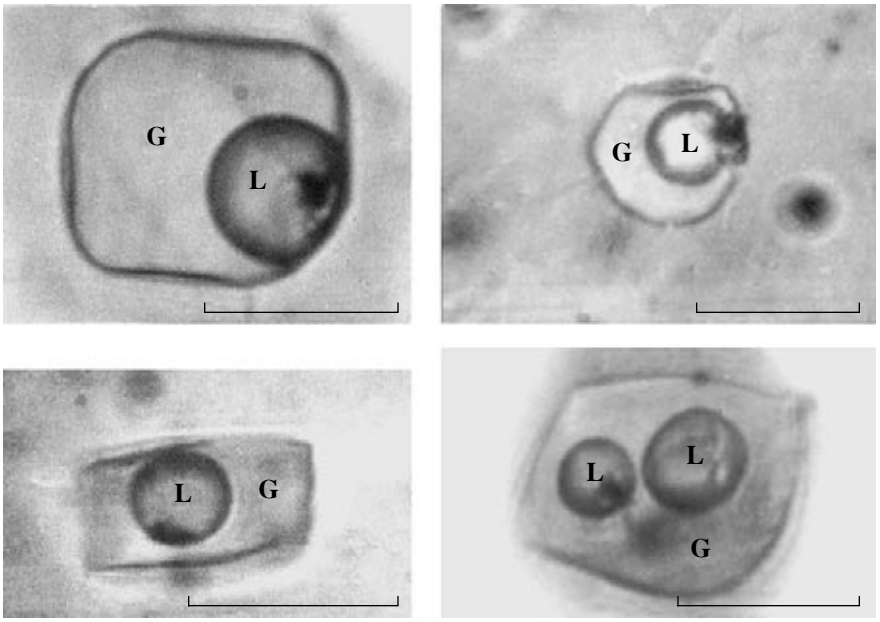

Fig. 3. Melt inclusions with a high-density water phase in plagioclase phenocrysts from the andesites of the Stiavnica stratovolcano. G is silicate glass and L, aqueous fluid. The scale bar is 20 μm.

RESULTS OF THE INVESTIGATIONS OF MELT AND FLUID INCLUSIONS IN MINERALS OF IGNEOUS ROCKS

Inclusions in Minerals of Andesites

Primary fluid and silicate melt inclusions occur in the central parts of plagioclase phenocrysts from the andesites. The fluid inclusions are 1–29 μm in size; they show negative crystal shapes and are composed of almost pure CO_2 (melting temperature from –56.9 to –56.6°C), which homogenizes to a gas phase at +18.8/30.1°C (densities of 0.19–0.35 g/cm^3 and pressures of 0.44–1.1 kbar at 800–1000°C). The silicate melt inclusions with a low-density gas vesicle were homogenized at temperatures of 1220–1150°C.

Peculiar inclusions were found in the outer growth zones of the plagioclase phenocrysts (Fig. 3). They are

Table 1. Chemical compositions (wt %) of homogenized melt inclusions in plagioclase from the andesites of the Stiavnica caldera (1–3), quartz from the rhyolites of the Vyhne extrusive dome (4–9), and quartz from the rhyolites of the Klotilda dike (10–13)

Component	1	2	3	4	5	6	7	8	9	10	11	12	13
SiO_2	68.94	67.19	65.02	75.60	71.24	71.52	74.20	74.71	74.23	76.54	75.94	75.44	70.59
SiO_2	0.09	0.08	0.08	0.05	0.08	0.06	0.04	0.06	0.01	0.07	0.03	0.02	0.04
Al_2O_3	13.17	12.88	12.50	8.48	13.34	13.08	12.12	11.77	10.02	11.16	10.88	10.73	12.61
FeO	0.90	0.88	0.85	0.64	0.59	0.72	0.57	0.71	0.54	0.81	0.69	0.77	0.55
MnO	0.04	0.04	0.04	0.00	0.05	0.05	0.02	0.04	0.08	0.05	0.06	0.05	0.10
MgO	0.13	0.12	0.12	0.07	0.05	0.08	0.05	0.02	0.06	0.06	0.03	0.04	0.03
CaO	1.40	1.39	1.38	0.57	0.97	0.99	0.95	0.80	0.62	0.74	0.68	0.71	0.76
Na_2O	2.46	2.45	2.45	3.63	4.77	3.46	3.96	4.19	3.75	1.11	1.60	1.63	1.85
K_2O	5.58	5.42	5.22	3.71	4.79	4.70	4.80	4.44	4.48	4.25	4.25	4.25	5.06
Cl	0.32	0.39	0.46	0.15	0.16	0.20	0.19	0.14	0.15	0.26	0.26	0.28	0.20
Total	93.03	90.84	88.12	92.90	96.04	94.86	96.90	96.88	93.94	95.05	94.42	93.93	91.79
H_2O*	7.06	9.27	12.00	7.10	3.96	5.14	3.10	3.12	6.06	4.95	5.58	6.07	8.21
T, °C	–	–	–	1050	970	970	960	940	900	790	810	800	650

* Water content in melts was determined by the method of [33] (analyses 1–3) and as a difference between 100% and the total of components in electron microprobe analyses (4–13).

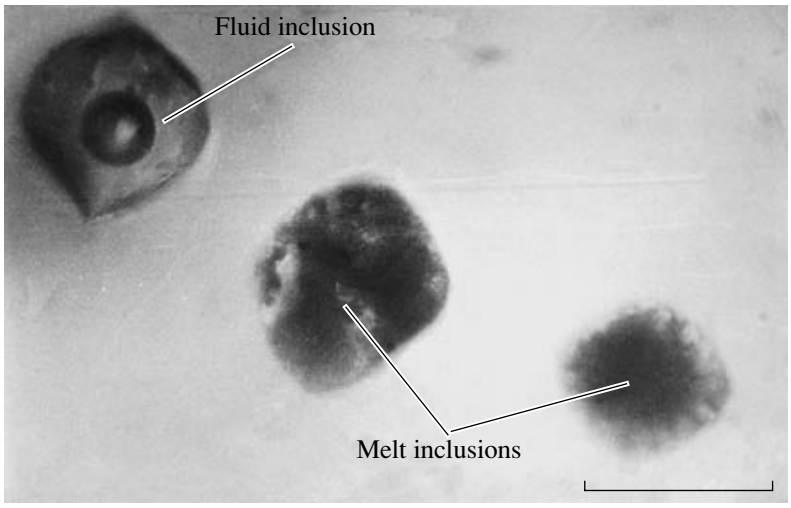

Fig. 4. Cogenetic silicate melt inclusions and an aqueous fluid inclusion in quartz phenocryst from the rhyolite of the Vyhne extrusive dome. The scale bar is 40 μm.

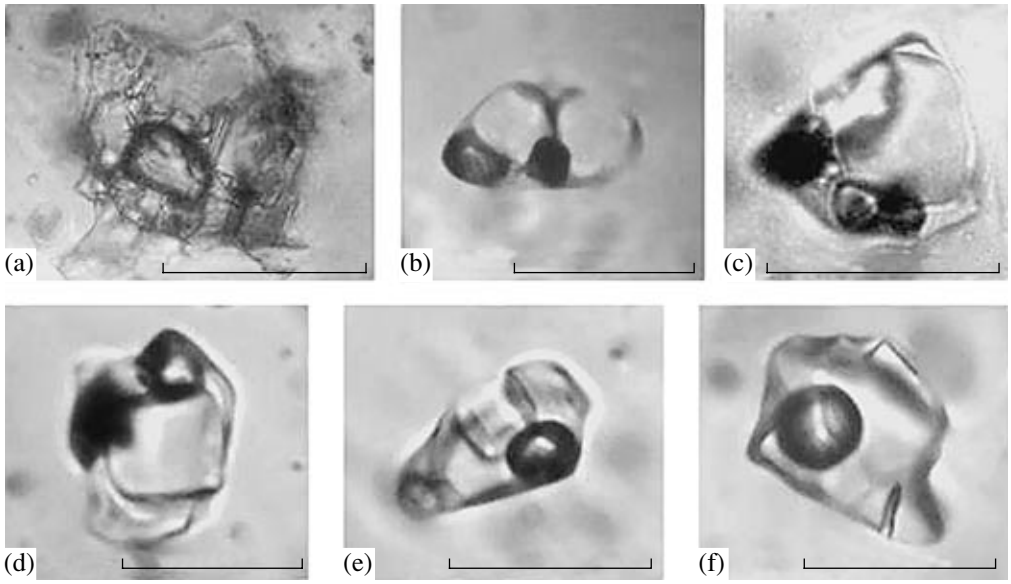

Fig. 5. Melt and fluid inclusions in quartz from the granodiorites of the Stiavnica–Hodrusa intrusive complex. (a) Inclusion of crystallized silicate melt. (b) Chloride melt inclusion with opaque phases, T_{hom} = 640°C. (c) Chloride melt inclusion with opaque phases, T_{hom} = 620°C. (d) Inclusion of chloride solution, T_{hom} = 510°C. (e) Inclusion of chloride solution, T_{hom} = 400°C. (f) Two-phase inclusion with T_{hom} = 267°C and a salinity of 6.6 wt % NaCl equiv. The scale bar is 20 μm.

from 2–3 to 62 μm in size and consist of silicate glass and a high-density fluid phase. The fluid phase is an aqueous solution with a salinity of 0.9–11.5 wt % (4.5 wt % on average) and a density of 0.79–1.08 g/cm^3 (1.03 g/cm^3 on average). The chemical analyses of the melt inclusions (Table 1, analyses 1–3) show high concentrations of SiO_2 (65.0–68.9 wt %), K_2O (up to 5.6 wt %), and Cl (up to 0.46 wt %) and low concentrations of TiO_2, MgO, and CaO. Pressure was estimated as 5.6–17 kbar for temperatures of 800–900°C, and the content of water in the melt was estimated as 7.1–12.0 wt %. These inclusions were described in detail elsewhere [32, 33].

Inclusions in Minerals of Rhyolites

Silicate melt inclusions and cogenetic inclusions of magmatic aqueous fluid were found in quartz and sanidine from the rhyolite of the extrusive dome near the village of Vyhne (Fig. 4). The melt inclusions were homogenized at 870–1050°C. The compositions of the homogenized melt inclusions (Table 1, analyses 4–9)

Table 2. Results of the estimation of water pressure, and concentrations of H_2O and Cl in silicate magmatic melts on the basis of inclusions in quartz from the granodiorites of the Stiavnica-Hodrusa intrusive complex (1–6) and quartz from the rhyolites of the Klotilda dike (7–9)

Parameter	1	2	3	4	5	6	7	8	9
T_1, °C	260	260	260	300	275	314	392	343	344
T_2, °C	–5.3	–5.7	–6.3	–5.5	–5.3	–16.1	–6.0	–6.9	–3.8
C_1, wt %	8.3	8.8	9.6	8.6	8.4	19.5	9.2	10.4	6.2
d, g/cm^3	0.86	0.87	0.88	0.80	0.85	0.90	0.64	0.76	0.70
V_1, vol %	18.1	16.6	19.1	13.9	16.9	18.0	6.9	12.0	10.3
V_2, vol %	81.9	83.4	81.9	86.1	83.1	82.0	93.1	88.0	89.7
dP/dT, bar/°C	11.3	10.8	10.6	9.9	10.5	9.8	11.3	8.7	8.2
P, kbar	3.8	3.7	3.6	3.0	3.4	2.9	2.4	3.1	2.8
m_1, g	15.57	14.44	15.93	11.12	14.37	16.20	4.42	9.12	7.21
m_2, g	14.27	13.17	14.40	10.16	13.16	13.04	4.01	8.17	6.76
m_3, g	0.78	0.76	0.92	0.58	0.72	1.90	0.25	0.57	0.27
m_4, g	221.1	225.2	221.1	232.5	224.4	221.4	223.4	211.2	215.3
m_5, g	–	–	–	–	–	–	13.41	17.11	17.22
m_6, g	236.7	239.6	237.1	243.6	238.7	237.6	227.9	220.3	222.5
C_2, wt %	6.0	5.5	6.1	4.2	5.5	5.5	7.6	11.5	10.8
C_3, wt %	0.33	0.32	0.39	0.24	0.30	0.80	0.34	0.52	0.38
n	3	4	3	2	5	3	2	4	5

Note: The calculations were performed by the method of [28]. T_1 is the homogenization temperature of fluid of the melt inclusion to a liquid phase; T_2 is the melting temperature of ice in the fluid phase of the melt inclusion; C_1 is the salinity of the fluid phase; d is the density of the fluid phase; V_1 is the volume of the fluid phase; V_2 is the volume of the silicate phases (glass in analyses 7–9); dP/dT is the pressure increase per 1°C temperature rise for the homogeneous fluid; P is the pressure of water fluid at a temperature of 600°C (analyses 1–6) or 680°C (analyses 7–9); m_1 is the mass of the fluid phase of the melt inclusion; m_2 is the mass of water in the fluid phase of the melt inclusion; m_3 is the mass of chlorine in the fluid phase of the melt inclusion; m_4 is the mass of silicate phases (analyses 1–6) or silicate glass (analyses 7–9) in the melt inclusion; m_5 is the mass of water in the silicate glass estimated from experimental solubility data [36] at calculated pressures of 2.4 kbar (analysis 7), 3.1 kbar (analysis 8), and 2.8 kbar (analysis 9); m_6 is the total mass of the melt inclusion (silicate phases + fluid phase); C_2 is the concentration of water in the silicate melt; C_3 is the concentration of chlorine in the silicate melt; and n is the number of inclusions in the given group. The following parameters were used in the calculations: the density of silicate phases in melt inclusions is 2.7 g/cm^3 (analyses 1–6), the density of water-saturated glass is 2.4 g/cm^3 (analyses 7–9), and the concentration of chlorine in felsic silicate glass is 0.25 wt % (electron microprobe data, Table 1). The temperatures of complete homogenization of the silicate inclusions are 800°C (analysis 7), 810°C (analysis 8), and 790°C (analysis 9).

are characterized by low TiO_2 and MgO concentrations, prevalence of K_2O over Na_2O, and rather high Cl contents (0.14–0.20 wt %). Judging from the total of components, the melt probably contains 3–7 wt % water. The primary inclusions of magmatic fluid homogenized to a liquid phase at 125–320°C and contain aqueous solution with a concentration of 1.7–3.9 wt %. The density of the fluid is 0.69–0.94 g/cm^3, which corresponds to a pressure of 3.3–8.7 kbar at 700–850°C. The inclusions often contain an opaque phase accounting for 0.5–0.1% of the total volume. Secondary fluid inclusions were never observed in the phenocrysts of rhyolites, which is indicative of the absence of hydrothermal alteration of these rocks. The investigations of these inclusions were reported in more detail in [34, 35].

Primary melt inclusions composed of a gas bubble and crystallized glass, which began to melt during heating at temperatures of 640–650°C, were found in quartz from the rhyolite of the Klotilda dike. After quenching, a meniscus of aqueous solution was observed in the fluid phase of these inclusions. Its homogenization to a liquid phase was observed at 343–392°C. The concentration of salts in the aqueous solution is 6.2–10.4 wt %. The complete homogenization of the melt inclusions was attained at 790–810°C. The concentrations of water and chlorine in the melt are rather high: 7.6–11.5 wt % H_2O and 0.34–0.52 wt % Cl (Table 2, analyses 7–9). The electron microprobe analysis of the homogenized inclusions (Table 1, analyses 10–13) showed that the felsic melts (76.5–75.4 wt % SiO_2) have low concentrations of TiO_2, FeO, MgO, and CaO and elevated concen-

Table 3. Results of investigations of fluid inclusions in quartz from the granodiorites of the Stiavnica-Hodrusa intrusive complex (1–5) and quartz from the rhyolites of the Klotilda dike (6–8)

Analysis no.	Temperature, °C				Salinity, wt % NaCl equiv.	Pressure, kbar	Density, g/cm^3	n
	T_1	T_2	T_3	T_4				
1	247–235	–70/–52	–	640–620	79.7–76.6	4.0–3.6	1.61–1.58	9*
2	270–265	–59	–	560–535	68.2–64.6	2.9–2.7	1.26–1.12	6
3	390–215	–63/–51	–	520–280	62.5–36.7	1.5–0.22	1.19–1.09	26
4	265–230	–59/–47	–	245/–5.1	34.4–28.6	0.11	1.11–1.00	19
5	370–225	–61/–35	–26.8/–0.8	–	27.1–1.4	–	1.04–0.77	54
6	587	–55	–19.4	–	22.0	–	0.51	2
7	356–302	–55/–51	–	560–465	67.7–55.2	2.2–1.6	1.25–1.12	18
8	472–233	–31	–20.6/–0.7	–	22.8–1.2	–	0.69–0.95	38

Note: T_1 is the temperature of homogenization to a gas phase; T_2 is the eutectic temperature; T_3 is the temperature of ice melting; T_4 is the temperature of halite dissolution; and n is the number of inclusions analyzed.

*Primary inclusion, all the other inclusions are secondary.

trations of K_2O (up to 5.1 wt %), Cl (up to 0.28 wt %), and H_2O (up to 8.2 wt %).

Inclusions in Quartz of Granodiorites

Primary silicate melt inclusions in quartz from the granodiorites of the Stiavnica–Hodrusa complex (Fig. 5a) are from 3 to 35 μm in size and contain anisotropic crystals of silicate minerals, aqueous Na–Mg chloride solution (eutectic temperatures range from –38 to –34°C) with a salinity of 8.3–19.5 wt % NaCl equiv., and a gas bubble disappearing at 260–314°C (homogenization to a liquid phase). Upon heating above 500°C, many of the inclusions decrepitated, which is indicative of a high internal pressure. Only a few very small inclusions were homogenized at 680–750°C. It is possible that there are inclusions with higher homogenization temperatures. Aqueous fluid pressure was estimated using the method of Naumov [28] for the temperature of the beginning of silicate phase melting (600°C) as 2.9–3.8 kbar, the concentration of water in the melt is 4.2–6.1 wt %, and that of chlorine is 0.24–0.80 wt % (Table 2, analyses 1–6).

The same quartz grains contain primary inclusions of chloride brine from 5 to 30 μm in size cogenetic with the silicate melt inclusions (Figs. 5b, 5c). They bear several isotropic phases (60–70 vol %), the largest of which has an index of refraction similar to that of quartz (i.e., this is halite), a gas bubble (10–15 vol %), an opaque phase (1–3 vol %), and aqueous solution (15–24 vol %). The cogenetic character of the inclusions is confirmed by the rare cases of coexistence of both inclusion types in the same growth zones of magmatic quartz. The inclusions of salt melts were also extensively decrepitated during heating. Some inclusions were homogenized at 618–640°C, and NaCl was the last to dissolve before the homogenization, whereas the gas bubble disappeared at 235–247°C, which implies a salt concentration of 77–80 wt % NaCl equiv. and a pressure of 3.6–4.0 kbar (Table 3).

Secondary inclusions in quartz of the granodiorites are represented by polyphase, three-phase with halite, and two-phase inclusions (Figs. 5d–5f). Their investigation revealed a gradual decrease in all parameters: homogenization temperature from 560 to 225°C, solution salinity from 68.2 to 1.5 wt % NaCl equiv., and pressure from 2.9 to 0.1 kbar (Table 3). The secondary inclusions in quartz of the granodiorites probably recorded gradual changes in the *P–T–X* parameters of fluid during transition from the magmatic stage to hydrothermal processes. The fluid salinity declines initially along the saturation curve, but it decreases more rapidly within the temperature interval 370–260°C, which could be related to the entrainment into the hydrothermal system of low-salinity vadose water, which diluted the magmatic fluid.

Secondary inclusions of postmagmatic fluid in quartz from the rhyolites of the Klotilda dike (Table 3, analyses 6–8) show considerable variations in both fluid salinity (67.7–1.2 wt %) and homogenization temperature (590–230°C).

Inclusions in Minerals of Basanites

High-density CO_2 fluid inclusions were found in phenocrysts from the Kalvari basanite neck among silicate melt inclusions (49 wt % SiO_2). The temperature of their homogenization to a liquid phase (18°C) corresponds to a CO_2 density of 0.80 g/cm^3. The most probable temperature of basanite magma is 1200°C, which implies a CO_2 pressure of 5.0 kbar. Taking into account a lithostatic pressure gradient of 280 bar/km, this pres-

Table 4. Results of the investigation of fluid inclusions in quartz, sphalerite, and carbonate from vein ores of the deep zone of the gold-silver mineralization of the Svyatozar vein system

Vein	Sample no.	Mineral	*n*	Temperature, °C			*C*	*P*, bar	*d*, g/cm^3
				T_1	T_2	T_3			
Laura	La-9/99 (206)	Quartz*	10	285–279	–22	–0.7	1.2	70–60	0.74–0.75
Laura	La-6/99 (206)	Quartz	21	270–267	–24	–1.7	2.9	–	0.79–0.80
Luisa	Lu-3/99 (217)	Quartz	5	310–296	–24	–1.2	2.1	–	0.70–0.73
Natalie	Na-34/97 (290)	Quartz*	25	313–269	–22	–1.2/–2.0	2.1–3.4	100	0.74–0.80
Natalie	Na-17/97 (268)	Quartz	32	275–255	–25/–21	–0.7/–0.8	1.2–1.4	–	0.76–0.79
Erika	Er-27/97 (268)	Quartz*	19	331–316	–22	–1.3	2.2	130–100	0.65–0.69
Magda	Mag-25/97 (290)	Quartz	63	278–271	–21/–22	–0.4/–1.2	0.7–2.1	–	0.75–0.81
Andrea	An 7/97 (268)	Quartz*	17	300–299	–23/–26	–1.0/–0.4	1.7–0.7	80	0.71–0.70
Andrea	An 7/97 (268)	Sphalerite	58	258–193	–38/–27	–1.3/–2.7	2.2–4.5	–	0.81–0.91
Andrea	An 7/97 (268)	Sphalerite	43	216–162	–35/–29	–2.4/–0.6	4.0–1.1	–	0.88–0.92
Christina	KR 4/97 (268)	Quartz*	5	348 (g)	–35	–0.3	0.5	160	n.d.
Christina	KR 4/97 (268)	Quartz*	114	328–250	–34/–22	–5.0/–0.3	6.5–0.5	120–50	0.55–0.84
Rozalia	Roz-57 (239)	Quartz	11	285–164	–38/–32	–1.4/–0.3	2.4–0.5	–	0.76–0.91
Rozalia	Roz-57 (239)	Sphalerite	2	280–266	–34	–1.8	3.0	–	0.77–0.80
Rozalia	Roz-57 (239)	Quartz	36	365–228	–40/–29	–5.1/–0.3	8.0–0.5	–	0.68–0.83
Rozalia	Roz-58 (239)	Quartz	7	326–276	–33/–32	–2.2/–1.2	3.7–2.0	–	0.71–0.77
Rozalia	Roz-58 (239)	Carbonate	14	310–210	–44/–25	–4.4/–0.5	7.0–0.9	–	0.78–0.86

Note: Numerals in parentheses after the sample numbers indicate absolute elevations above the sea level in meters. The minerals marked by asterisks contain inclusions with evidence for fluid unmixing (boiling). *n* is the number of inclusions studied, T_1 is the homogenization temperature, T_2 is the eutectic temperature, T_3 is the temperature of ice melting, *C* is the salinity of solution in wt % NaCl equiv., *P* is the pressure, *d* is the fluid density, and (g) denotes homogenization of fluid inclusions to a gas phase (others homogenized to a liquid phase).

sure corresponds to a depth of inclusion entrapment of 18 km. Thus, already at such great depths, CO_2 occurred as a separate fluid phase.

RESULTS OF THE INVESTIGATION OF FLUID INCLUSIONS IN THE MAIN TYPES OF EPITHERMAL MINERALIZATION

Deep Subepithermal Au Mineralization of the Svyatozar Vein System

We studied 412 individual fluid inclusions in quartz and sphalerite from nine samples collected in the Andrea, Cristina, Laura, Luisa, Magda, Natalie, and Erika veins, which represent mainly the gold-producing stage of mineralization. The fluid inclusions are large (15–150 μm), sometimes have negative crystal shapes, and are often confined to growth zones (evidence for their primary nature). Groups of cogenetic inclusions were frequently found homogenizing at similar temperatures both to liquid and gas phases, which demonstrates the existence of heterogeneous fluid. The results of the thermometric and cryometric investigations of these inclusions are given in Table 4. The table also shows the results reported by M. Kalinai [26] on 70 fluid inclusions in quartz, sphalerite, and carbonate from three samples from the Rozalia vein. Most of these inclusions characterize an early gold-free stage.

Ore minerals were precipitated from hot Na–Mg chloride solutions with salt concentrations of 0.5–8.0 wt % NaCl equiv. at temperatures of 330–160°C in open fractures at low pressures, often from boiling solutions (in such a case, no pressure correction is needed to homogenization temperatures). Pressure was estimated for the cases of boiling, mainly from water vapor pressure as 60–130 bar. The presence of CO_2 and Cl in the solutions of inclusions was supported by the data of ion and gas chromatography (Table 5). In addition, these analyses revealed small contents of nitrogen (0.01 mol %), SO_4^{2-}, and F^- in the ore-forming fluids.

Epithermal Au–Ag–Pb–Zn Vein Mineralization in the Terezia, Bieber, Spitaler, Viliam, and Rozalia Vein Systems

We studied more than 2000 fluid inclusions in quartz, sphalerite, barite, carbonate, and fluorite from 100 samples, representing mainly the gold–base metal stage of mineralization. The results of the thermometric

Table 5. Results of the analysis of fluid inclusions by ion and gas chromatography

Sample no.	Mineral	Vein	Na^+	K^+	F^-	Cl^-	SO_4^{2-}	H_2O	CO_2	CH_4	N_2
			mol/kg H_2O					mol %			
Te-61/88a	Quartz	Terezia	–	–	0.11	0.13	0.01	99.45	0.55	0.00	0.00
Te-61/88b	″	″	–	–	0.02	0.05	0.00	99.78	0.21	0.00	0.01
Te-1/92a	″	″	0.09	0.06	0.17	0.02	0.02	99.39	0.59	0.00	0.02
Te-7/92	″	″	0.02	0.01	0.02	0.01	0.01	99.70	0.29	0.00	0.01
W-7/93a	″	″	–	–	0.25	0.17	0.01	98.22	1.73	0.05	0.00
W-7/93b	″	″	–	–	0.03	0.05	0.01	98.52	1.45	0.00	0.03
W-11/93a	″	″	–	–	0.03	0.12	0.01	99.48	0.52	0.00	0.00
W-11/93b	″	″	–	–	0.06	0.05	0.01	98.81	1.16	0.00	0.03
W-20/93a	″	″	–	–	0.01	0.07	0.01	99.31	0.66	0.03	0.00
W-20/93b	″	″	–	–	0.01	0.03	0.00	99.73	0.27	0.00	0.00
Te-II-3	″	″	0.36	0.05	0.00	0.24	0.05	99.69	0.30	0.00	0.01
Te-II-11	″	″	–	–	0.09	0.07	0.05	98.87	1.10	0.01	0.02
Te-II-III-1a	″	″	0.17	0.13	0.00	0.22	0.05	97.75	1.53	0.03	0.69
Te-VIII-2	″	″	–	–	0.02	0.11	0.01	91.58	8.37	0.00	0.05
Te-43/88a	″	″	0.21	0.05	0.08	0.37	0.02	92.66	7.34	0.00	0.00
Bi-17/89	″	Bieber	0.37	0.10	0.45	0.12	0.25	99.70	0.29	0.00	0.01
Bi-8/89	″	″	0.30	0.06	0.01	0.15	0.09	99.81	0.18	0.00	0.01
Bi-9/89	Sphalerite	″	0.53	0.07	0.08	0.63	0.07	99.11	0.89	0.00	0.00
Bi-37/89	Quartz	″	0.18	0.03	0.02	0.12	0.02	99.67	0.32	0.00	0.01
Bi-47/89	″	″	0.24	0.03	0.00	0.22	0.21	99.75	0.25	0.00	0.00
Bi-53/89	″	″	0.22	0.02	0.06	0.13	0.32	99.86	0.14	0.00	0.00
Bi-19/89	Sphalerite	″	–	–	0.08	0.63	0.07	99.10	0.89	0.00	0.01
Bi-14/89	Quartz	Spitaler	0.37	0.05	0.19	0.24	0.01	99.89	0.11	0.00	0.00
Bi-16/89	″	″	–	–	0.18	0.16	0.01	99.70	0.29	0.00	0.01
Bi-11/89a	″	″	0.10	0.01	0.00	0.06	0.03	99.88	1.12	0.00	0.00
Bi-11/89b	Sphalerite	″	0.33	0.15	0.02	0.14	–	95.99	3.16	0.00	0.85
Sp-IX-1	Barite	″	0.18	0.04	0.37	0.14	–	93.87	6.08	0.02	0.03
Sp-XII-1	Quartz	″	0.45	0.05	0.01	0.24	0.02	99.70	0.29	0.00	0.01
Sp-XII-1b	Sphalerite	″	0.41	0.10	0.00	0.19	0.00	96.51	3.47	0.00	0.02
Lu-XV-3/99	Quartz	Svyatozar	–	–	0.01	0.06	0.00	99.64	0.36	0.00	0.00
Na-XIII-34	″	″	–	–	0.05	0.06	0.01	99.85	0.14	0.00	0.01
Na-XIII-34a	″	″	–	–	0.02	0.10	0.01	99.79	0.20	0.00	0.01
Mg-XII-25	″	″	–	–	0.01	0.08	0.00	99.90	0.09	0.00	0.01
Er-XII-27	″	″	–	–	0.01	0.12	0.02	99.83	0.16	0.00	0.01

and cryometric investigations of individual inclusions are shown in Table 6 and Figs. 6–8.

Fluid inclusions containing mineral-forming solutions that produced the Au–Ag and Au–Ag–base metal mineralization of the Terezia vein system were characterized most thoroughly. We investigated 950 individual inclusions in quartz, sphalerite, and barite from 51 samples representing the Au–Ag sulfide-poor type of mineralization of the upper level (600 m above sea level), the Au–Ag–base metal type of mineralization of the middle level (between 600 and 100 m above sea level), and the mainly base-metal type of mineralization of the lower level (below 100 m above sea level). The middle and lower levels of the development of Au–Ag–Bi–Cu–Pb–Zn mineralization in the Bieber vein system were characterized using 20 samples (790 fluid inclusions); and the middle level of mainly base-metal mineralization in the Spitaler vein system was represented

Table 6. Results of the investigation of fluid inclusions in minerals from the ore veins of epithermal mineralization in the Banska Stiavnica deposit

Sample no.	Mineral	*n*	Temperature, °C			*C*, wt % NaCl equiv.	*P*, bar	*d*, g/cm^3
			T_1	T_2	T_3			
Terezia vein system								
Te-X (790)	Quartz*	27	275–265	–32/–29	–2.0/–1.2	3.4–2.1	60–50	0.81–0.78
Te-55/89 (790)	Quartz*	49	305–244	–35/–31	–2.6/–0.4	4.3–0.7	90–40	0.85–0.70
Te-62/88 (790)	Quartz*	54	310–200	–37/–31	–5.1/–2.9	8.0–4.8	30–20	0.92–0.78
Te-1/92 (730)	Quartz*	35	301–240	–23/–10	–1.6/–0.2	2.7–0.4	40–30	0.82–0.71
Te-2/92 (730)	Quartz	12	310–175	–22/–17	–1.3/–0.9	2.2–1.6	–	0.91–0.71
W-2/95 (730)	Sphalerite	22	294–248	–37/–36	–6.7/–1.9	10.1–3.2	–	0.85–0.83
W-4/95 (730)	Quartz*	52	289–267	–25/–21	–6.9/–1.0	10.4–1.7	70–60	0.86–0.74
W-5/95 (730)	Quartz	27	287–270	–26/–25	–2.6/–2.1	4.3–3.6	–	0.81–0.77
W-7/95 (730)	Sphalerite	7	220	–32	–2.2	3.7	–	0.87
W-7/95 (730)	Quartz	11	278–272	–25	–0.4	0.7	–	0.75
Te-5/92 (730)	Quartz	17	275–151	–26/–23	–0.5/–0.4	0.9–0.7	–	0.92–0.75
Te-4/92 (730)	Quartz*	32	322–214	–27/–22	–1.2/–0.2	2.1–0.4	100–70	0.85–0.69
Te-12/92 (730)	Quartz	6	267	–33	–1.3	2.2	–	0.79
W-7 (730)	Sphalerite	1	296	n.d.	–1.7	2.9	–	0.74
W-11 (730)	Quartz	6	299–250	n.d.	–2.0/–1.4	3.4–2.4	–	0.81–0.73
W-20 (730)	Sphalerite	1	250	n.d.	–3.6	5.9	–	0.84
W-20 (730)	Quartz	1	255	n.d.	–3.4	5.6	–	0.83
Te-I/7 (630)	Quartz	1	314	–28	–1.9	3.2	–	0.71
Te-II/3 (555)	Quartz*	20	294–171	–34/–31	–3.2/–0.4	5.2–0.7	70–50	0.93–0.72
Te-II/3 (555)	Sphalerite	3	261–228	–34	–2.3	3.9	–	0.87–0.82
Te-II/9 (555)	Quartz	4	249–213	–39/–33	–1.9/–0.9	3.2–1.6	–	0.86–0.82
Te-II/22 (555)	Quartz	5	337–246	–36/–33	–2.5/–0.1	4.2–0.2	–	0.82–0.69
Te-II/22 (555)	Sphalerite	1	238	–45	–3.5	5.7	–	0.86
Te-22/88 (555)	Quartz*	27	260–224	–36/–31	–2.0/–1.0	3.4–1.7	50–40	0.85–0.82
Te-30/88 (555)	Quartz*	34	293–244	–37/–31	–2.2/–0.6	3.7–1.0	70–60	0.83–0.74
Te-32/88 (555)	Sphalerite	30	280–157	–37/–31	–3.4/–1.8	5.5–3.1	–	0.95–0.78
Te-35/88 (555)	Quartz*	49	290–210	–36/–31	–4.4/–0.9	7.0–1.6	70–20	0.90–0.75
Te-II-III/10 (530)	Quartz*	34	293–155	–35/–30	–7.7/–0.8	11.4–1.4	70–20	0.97–0.73
Te-V-1 (430)	Barite	14	201–50	–31/–30	–0.8/–0.4	3.1–0.7	–	1.00–0.89
Te-V-2 (430)	Sphalerite	5	275–255	–31/–29	–2.9/–2.7	4.8–4.5	–	0.84–0.81
Te-V-2 (430)	Quartz	2	266	–31	–0.8	1.4	–	0.79
Te-IX-2 (315)	Quartz*	9	305–251	–30/–28	–1.6/–0.5	2.7–0.9	90–60	0.81–0.74
Te-IX-7 (315)	Barite	18	205–50	–29	–2.4/–0.5	4.0–0.9	–	1.00–0.90
Te-IX-1 (315)	Sphalerite	11	279–259	–37/–36	–3.9	6.3	–	0.83–0.81
Te-IX-1 (315)	Quartz	12	294–138	–47/–35	–2.3/–0.7	7.3–1.2	–	0.98–0.76
Te-IX-1a (315)	Sphalerite	65	289–133	–39/–34	–6.8/–3.9	10.2–6.3	–	1.00–0.79
Te-IX-1 (315)	Quartz	96	307–160	–36/–30	–6.4/–2.6	9.7–4.3	90–60	0.98–0.75
Te-IX-1c (315)	Quartz	8	185–155	–37	–6.6	10.0	–	0.98–0.96
Te-43/88 (95)	Sphalerite	10	305–253	–36	–6.6/–3.1	10.0–5.1	–	0.84–0.83
Te-43/88 (95)	Quartz	11	211–165	–34/–32	–4.7/–3.2	7.4–5.2	–	0.95–0.90
Te-42/88 (95)	Sphalerite	15	308–292	–36	–3.9/–2.9	6.3–4.8	–	0.79–0.77
Te-42/88 (95)	Quartz	19	200–183	–34/–32	–3.1/–2.9	5.1–4.8	–	0.92–0.91
Te-48/88 (95)	Sphalerite	17	181–145	–38/–36	–5.9/–3.1	9.1–5.1	–	0.98–0.95
Te-44/88 (95)	Quartz	13	353–175	–36/–34	–5.7/–.36	8.8–5.8	–	0.96–0.69
Te-41/88 (95)	Sphalerite	56	301–273	–36/–32	–3.6/–3.1	5.8–5.1	–	0.81–0.78
Te-41/88 (95)	Quartz	15	229–222	–31	–1.1	1.9	–	0.85
Te-II-8/9 (95)	Quartz	17	320–175	–50	–8.3/–7.7	12.1–11.3	–	0.96–0.81
Te-II-14 (95)	Sphalerite	9	160–149	–31/–30	–3.1/–2.6	5.1–4.3	–	0.95
Te-V-2 (110)	Quartz	10	310–267	–38/–35	–6.4/–5.1	9.7–8.0	–	0.86–0.80
Te-V-2 (110)	Quartz	2	196–186	–37	–5.2	8.1	–	0.94
Te-V-2 (110)	Sphalerite	32	336–291	–38/–31	–6.4/–3.2	9.7–5.2	–	0.79–0.76

Table 6. (Contd.)

Sample no.	Mineral	n	Temperature, °C			C, wt % NaCl equiv.	P, bar	d, g/cm^3
			T_1	T_2	T_3			
Bieber vein system								
Bi-17/89 (480)	Sphalerite	35	267–190	–33/–29	–1.8/–1.0	3.1–1.7	–	0.89–0.80
Bi-3/89 (430)	Sphalerite	46	183–168	–36/–31	–2.9/–1.8	4.8–3.1	–	0.92–0.91
Bi-8/89 (430)	Quartz*	86	203–174	–35/–30	–2.6/–1.3	4.3–2.2	10	092–0.89
Bi-9/89 (430)	Quartz*	36	244–237	–33/–30	–3.1/–2.9	5.1–4.8	30–20	0.86–0.85
Bi-8/89 (430)	Sphalerite	50	253–241	–49/–45	–4.1/–2.5	6.6–4.2	–	0.87–0.83
Bi-37/89 (315)	Quartz*	77	294–267	–33/–31	–2.6/–1.1	4.3–1.9	70–50	0.79–0.77
Bi-44/89 (315)	Sphalerite	46	267–159	–38/–30	–3.2/–1.6	5.2–2.7	–	0.92–0.82
Bi-47/89 (315)	Quartz	24	280–135	–33/–27	–2.8/–0.6	4.6–1.0	–	0.93–0.78
Bi-47/89 (315)	Sphalerite	22	265–175	–36/–31	–2.6/–1.5	4.3–2.6	–	0.92–0.80
Bi-17/89 (315)	Sphalerite	6	198–191	–22/–21	–3.6/–1.4	5.9–2.4	–	0.91–0.90
Bi-49/89 (240)	Quartz*	52	378–245	–36/–31	–2.9/–2.4	4.8–4.0	240–40	0.83–0.62
Bi-49/89 (240)	Sphalerite	22	175–170	–36/–34	–2.3/–2.1	3.9–3.5	–	0.92
Bi-51/89 (240)	Quartz*	29	214–149	–33/–29	–1.8/–1.1	3.1–1.9	–	0.93–0.85
Bi-53/89 (240)	Sphalerite	15	214	–36	–2.6	4.3	–	0.88
Bi-53/89 (240)	Quartz	42	282–185	–36/–32	–2.8/–0.7	4.6–1.2	–	0.90–0.78
Bi-50/88 (95)	Sphalerite	29	192–172	–38/–35	–2.4/–1.5	4.0–2.6	–	0.91
Bi-51/88 (95)	Sphalerite	34	194–163	–37/–29	–3.2/–1.8	5.2–3.1	–	0.94–0.90
Bi-53/88 (95)	Quartz	21	281–184	–36/–31	–3.1/–0.3	5.1–0.5	–	0.88–0.80
Bi-53/88 (95)	Sphalerite	31	274–241	–37/–35	–3.2/–2.5	5.2–4.2	–	0.84–0.80
Bi-53/88 (95)	Quartz	21	309–204	–37/–31	–7.9/–3.9	11.6–6.3	–	0.92–0.82
Bi-56/88 (95)	Quartz	58	288–229	–37/–30	–3.1/–1.5	5.1–2.6	–	0.86–0.77
Bi-2-25/8 (95)	Sphalerite	34	212–141	–35/–27	–6.9/–4.0	10.4–4.5	–	0.95–0.92
Bi-2-43/8 (95)	Sphalerite	21	224–198	–27/–21	–4.2/–0.8	6.7–1.4	–	0.89–0.88
Spitaler vein system								
Bi-16/89 (480)	Quartz*	27	255–210	–34/–29	–3.1/–1.1	5.1–1.9	50–20	0.87–0.83
Bi-11/89 (430)	Quartz	22	245–205	–35/–32	–4.1/–3.3	6.6–5.4	–	0.91–0.84
Bi-12/89 (430)	Quartz	67	240–255	–39/–34	–2.3/–1.0	3.9–1.7	–	0.87–0.82
Bi-12/89 (430)	Sphalerite	25	270–230	–48/–43	–5.8/–4.7	8.9–7.4	–	0.91–0.84
Bi-13/89 (430)	Quartz	37	295–245	–37/–32	–3.1/–0.8	5.1–1.4	–	0.81–0.77
PS-5E (430)	Fluorite	8	204–150	–36/–33	–1.1/–1.0	1.9–1.7	–	0.93–0.87
PS-5E (430)	Sphalerite	15	175–165	–35/–31	–3.4/–2.8	5.5–4.6	–	0.94–0.93
Viliam vein system								
Bi-14/89 (490)	Quartz*	53	280–255	–34/–33	–3.5/–2.6	5.7–4.3	60–50	0.84–0.79
Bi-14/89 (490)	Sphalerite	45	275–270	–39/–35	–4.1/–1.6	6.6–2.7	–	0.79
Bi-15/89 (490)	Quartz	56	270–225	–35/–34	–4.1/–2.4	6.6–4.0	–	0.8–0.80
Rozalia vein system								
Roz-2/88 (392)	Quartz	18	302–269	–33/–30	–2.0/–1.3	3.4–2.2	–	0.79–0.75
Roz-10 (445)	Quartz*	7	190–150	–30	–2.5	4.2	10	0.95–0.91
Roz-43 (445)	Ametyst	35	324–147	–41/–21	–3.0/–1.0	4.9–1.7	–	0.94–0.72
Roz-21F (445)	Sphalerite	7	293–161	–45/–39	–5.1/–2.5	8.0–4.2	–	0.94–0.82
Roz-21F (445)	Quartz	24	313–118	–38/–27	–5.1/–1.4	8.0–2.3	–	0.94–0.78
Roz-Z-1 (239)	Sphalerite	9	293–125	–44/–35	–5.2/–1.6	8.1–2.7	–	0.96–0.82
Roz-Z-1 (239)	Quartz	10	340–269	–46/–43	–3.0/–1.4	4.9–2.4	–	0.79–0.68
Roz-9 (239)	Carbonate	10	302–264	–41–32	–4.0/–1.6	6.4–2.7	–	0.80–0.78
Roz-10 (239)	Quartz	8	330–290	–40/–29	–1.4/–0.8	2.4–1.4	–	0.73–0.66
Roz-10 (239)	Sphalerite	6	267–251	–42/–39	–1.8/–1.2	3.0–2.0	–	0.81–0.80
Roz-11 (239)	Quartz	19	345–281	–41/–31	–1.4/–0.5	2.4–0.9	–	0.74–0.62
Roz-11 (239)	Carbonate	3	308–300	–41/–38	–1.4/–1.2	2.4–2.0	–	0.72–0.71
Roz-27 (239)	Quartz	12	319–234	–40/–34	–5.3/–1.3	8.3–2.2	–	0.84–0.78
Roz-28 (239)	Sphalerite	6	232–151	–50/–44	–8.5/–6.4	12.3–9.7	–	0.99–0.93

Note: Numerals in parentheses after the sample numbers indicate the absolute elevations above the sea level in meters. The minerals marked by asterisks contain inclusions with evidence for fluid unmixing (boiling). n is the number of inclusions studied, T_1 is the homogenization temperature, T_2 is the eutectic temperature, T_3 is the temperature of ice melting, C is the salinity of solution, P is the pressure, d is the fluid density, and n.d. denotes not determined.

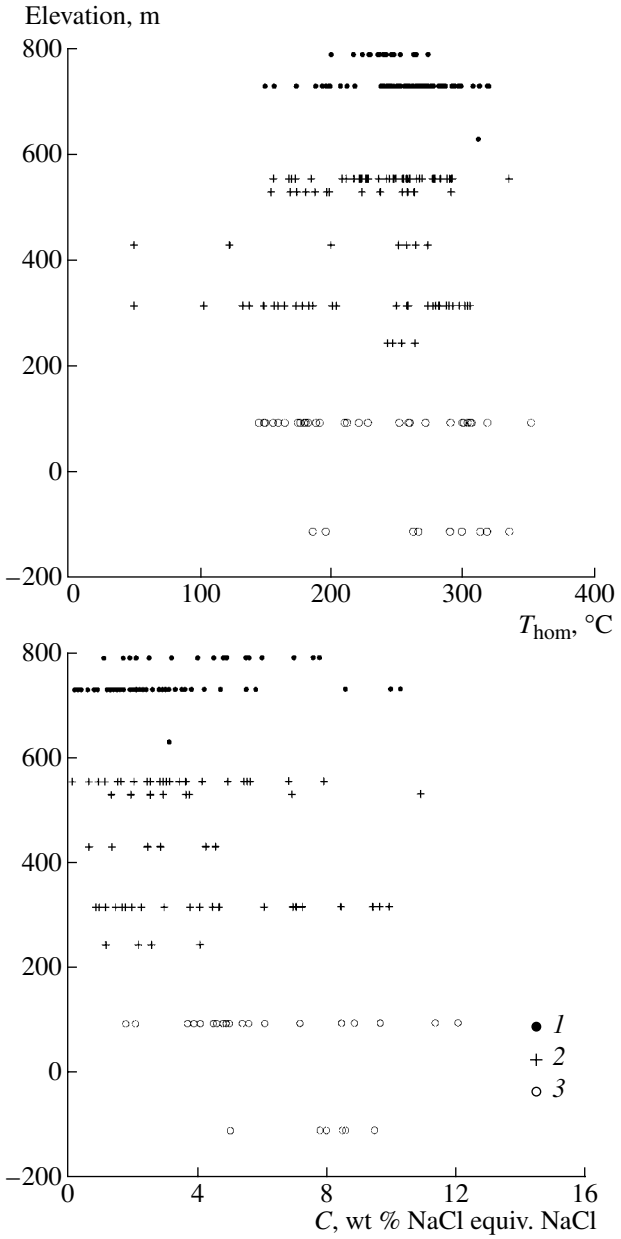

Fig. 6. Homogenization temperature (T_{hom}, °C) and salinity (*C*, wt % NaCl equiv.) of fluid inclusions in minerals of the Banska Stiavnica deposit as functions of altitude of sampling sites. (*1*) Upper levels (above 600 m), (*2*) middle levels (600–100 m), and (*3*) lower levels (below 100 m).

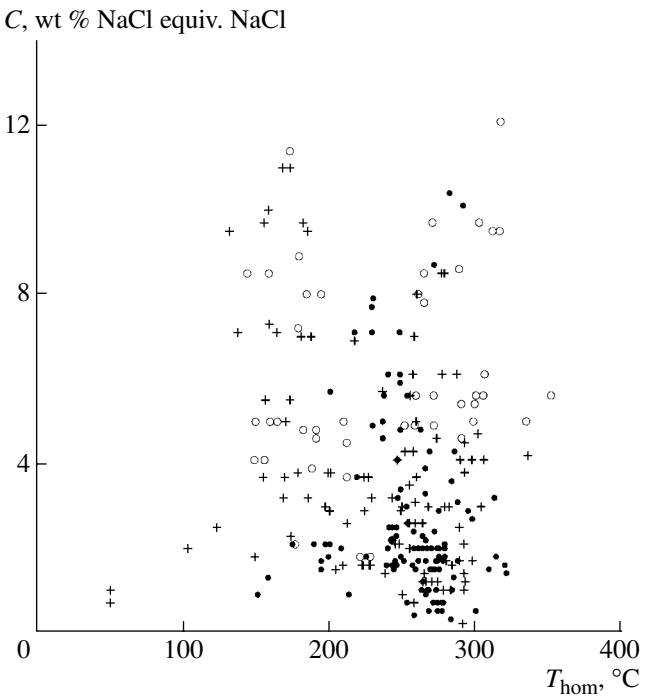

Fig. 7. Homogenization temperatures and salinities of fluid inclusions in minerals from the Banska Stiavnica deposit. Symbols are the same as in Fig. 6.

by nine samples (350 fluid inclusions). The characteristics of fluids responsible for the precipitation of Au–Ag–Bi–Cu and Pb–Zn–Cu mineralization in the middle levels of the Rozalia vein were mainly taken from Kalinai [26] (eight samples and 116 fluid inclusions). Thus, fluid inclusions were investigated within the whole vertical interval of almost 900 m of the development of ore mineralization.

In most samples reported in this paper (Table 6), we observed groups of cogenetic inclusions homogenized at similar temperatures to both liquid and gas phases, which is an indicator of the heterogeneous state (boiling) of fluids. The important role of fluid boiling during the formation of vein mineralization is also supported by the wide occurrence of brecciated structures in the veins. Boiling was documented at various temperatures during quartz crystallization up to a depth of 315 m in the Terezia vein, 95 m in the Bieber vein, 490 m in the Spitaler vein, and 445 m in the Rozalia vein, but was never observed in sphalerite, barite, fluorite, and calcite (Table 6).

Ores were deposited from high-temperature Na–Mg chloride solutions with salt concentrations of 0.2–12.1 wt % NaCl equiv., at temperatures of 380–50°C, in open fractures, at low pressure, often from boiling solutions, which do not require corrections to homogenization temperatures. Pressure was estimated for the cases of boiling, mainly from water vapor pressure (CO_2 pressure was no higher than 0.5–4.5 bar) as 10–240 bar. The homogenization temperatures of the majority of inclusions are 200–335°C, and pressures are 20–90 bar, which is typical of epithermal systems. The presence of CO_2 and Cl in the inclusion solutions was confirmed by ion and gas chromatography (Table 5). In addition, small amounts of nitrogen and methane and SO_4^{2-} and F^- ions were detected by these analyses.

The obtained pressure values allow us to estimate (very approximately) the depth of ore deposition. It is usually believed that the conditions of the beginning of

boiling in a hydrothermal system correspond to the maximum paleodepth. These conditions are characterized by the highest values of temperature and pressure in the given case. If pressure is assumed to be hydrostatic during ore deposition, which is valid for ore deposition in open fractures, the depth of formation of mineralization can be estimated as 1.6–0.8 km for the early stage and 1.1–0.4 km for the late stage. The spatial superposition of these stages allows us to suppose that the block hosting the mineralization was uplifted between the stages. Evidence for significant vertical movements has been reported from many caldera structures, including the Stiavnica stratovolcano [17, 25].

Near-Surface Epithermal Vein Au–Ag Mineralization in the Terezia and Bieber Vein Systems

Fluid inclusions in quartz and sphalerite of the ore veins are large (80–10 μm), have negative crystal shapes, and are often confined to growth zones (primary). There are numerous groups of cogenetic inclusions homogenizing at similar temperatures to liquid and gas phases, which is an indicator of the heterogeneous state of fluid. The results of thermometric and cryometric investigations of more than 300 individual inclusions are given in Table 6.

Ore precipitation occurred from hot Na–Mg chloride solutions with salt concentrations of 10.4–0.4 wt % NaCl equiv. at temperatures of 320–150°C, in open fractures, at low pressures, and often from boiling solutions. Pressure was estimated for the cases of boiling from water vapor pressure as 100–20 bar. The presence of CO_2 and Cl in the solutions of inclusions was confirmed by ion and gas chromatography (Table 5). In addition, chromatographic investigations revealed small amounts of nitrogen and methane and SO_4^{2-} and F^- ions in the ore-forming fluids.

Abundances of Metals in the Ore-Forming Fluids

The analysis of water extracts by the ICP MS method allowed us to determine the concentrations of a number of elements in solutions (in g/kg H_2O) (Table 7).

DISCUSSION AND CONCLUSIONS

The combined study of fluid inclusions allowed us to determine the main parameters and compositions of all types of endogenous fluid for the natural large-scale fluid–magma system of Banska Stiavnica. Magmatic fluids were explored from the intrusive (granodiorite), subvolcanic (rhyolites), and extrusive (andesites) levels, as well as postmagmatic hydrothermal fluids and ore-forming fluids of ore veins. The composition of magmatic melts evolved in the system from intermediate to felsic rocks, and the fluid regime changed concurrently.

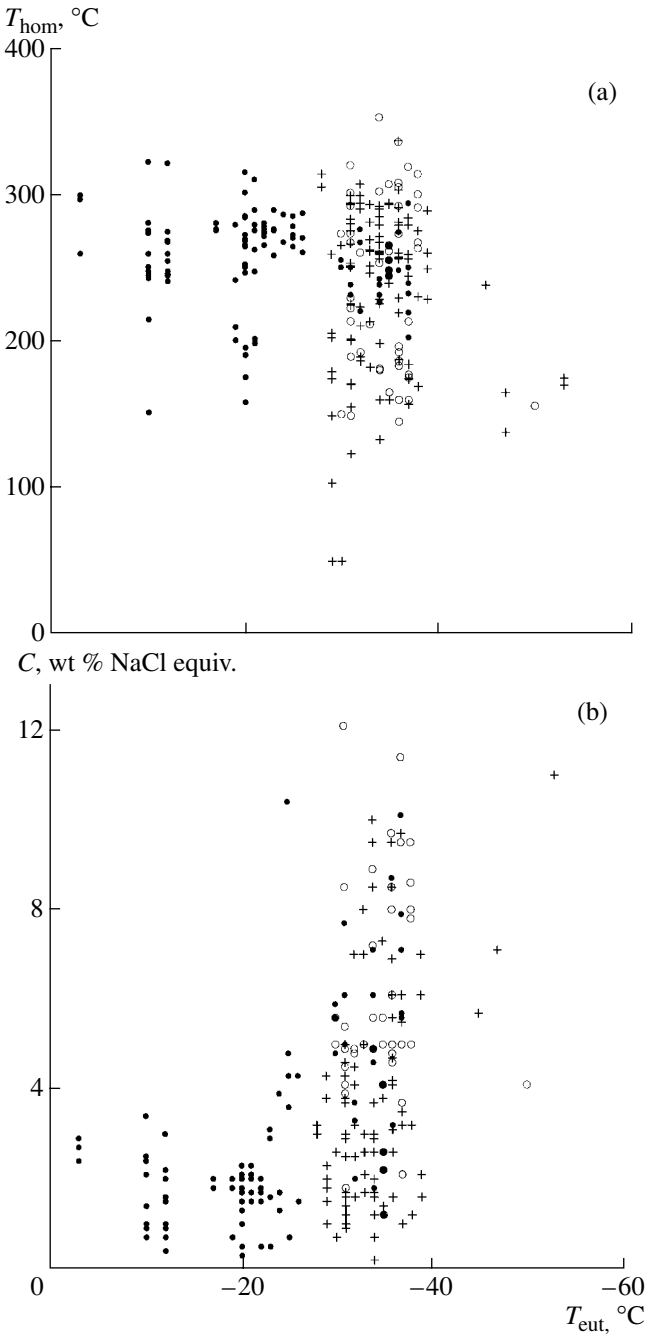

Fig. 8. Homogenization temperature and salinity of fluid inclusions in minerals from the Banska Stiavnica deposit as functions of the eutectic temperature of solutions from these inclusions. Symbols are the same as in Fig. 6.

Inclusions of silicate melt in the plagioclase phenocrysts of biotite–hornblende andesites were formed at temperatures of 1220–880°C and water fluid pressures from 17 to 5.6 kbar. The silicate melts (65–69 wt % SiO_2 and 5.2–5.6 wt % K_2O) showed high contents of water (7.1–12.0 wt %) and chlorine (0.32–0.46 wt %). The aqueous fluid is a salt solution with a moderate concentration (11.5–0.9 wt %) and a high density

Table 7. Concentrations (ppm) of selected elements in the solutions of fluid inclusions measured in water extracts by the ICP MS method

Element	Bi-8/89	Bi-17/89	Bi-37/89	Bi-16/89	Te-II-3	Hd-104/85
Li	44	248	–	66	120	1490
Mn	11	177	–	–	–	–
Co	11	10	1	2	8	48
Ni	200	250	3	22	170	300
Cu	580	550	3	190	740	1750
Ga	1.8	–	0.7	–	1.7	–
Se	–	–	–	–	360	–
Rb	75	190	49	50	89	210
Sr	440	–	94	180	530	1260
Ag	1.8	9.5	–	3	–	–
Cd	7	–	–	–	–	–
Cs	9	7	3	5	10	18
La	4	–	4.3	–	–	–
Ce	–	–	33	–	–	–
Pr	–	0.5	–	–	0.5	–
Nd	3.1	–	2.4	–	1.0	9.6
Eu	–	0.2	–	–	0.2	11
Tb	0.6	–	–	0.2	–	1.8
Dy	–	–	0.7	–	0.2	1.8
Ho	–	1.4	–	–	–	–
Er	–	4.1	–	–	1.7	–
Yb	–	0.5	–	0.2	–	7.8
Tl	–	–	–	–	5.8	–
Pb	180	330	7	24	73	–
U	–	–	–	–	–	18
Au	–	33	–	–	280	–

Note: Dashes denote concentrations below the detection limit of the analytical method.

(1.08–0.79 g/cm^3). On the other hand, the central parts of phenocrysts contain a low-density CO_2 fluid trapped at pressures of 1.1–0.44 kbar.

The inclusions of silicate melt in quartz phenocrysts from the subvolcanic rhyolites indicate high temperatures (1050–790°C), pressures (8.7–2.4 wt %), and water concentrations (11.5–3.1 wt %). Their magmatic fluid is represented by aqueous salt solution with a moderate concentration (3.9–1.7 wt %) and a high density (0.94–0.69 g/cm^3). The postmagmatic fluids trapped in secondary inclusions also show a wide range of temperatures (587–233°C) and a decrease in pressure (from 2.2 to 1.2 kbar) and salt concentration (from 68 to 1.2 wt %) with decreasing temperature.

Table 8. Concentrations of N_2 and CO_2 in fluid inclusions in phenocrysts from the rhyolites of the Vyhne extrusive dome and minerals from ore veins in the Banska Stiavnica deposit

Rock, vein	Mineral	*n*	Concentration, g/kg H_2O	
			N_2	CO_2
Rhyolite of the Vyhne dome	Quartz	2	9.5	57
	Sanidine	3	7.8	61
	Groundmass glass	1	0.16	–
Bieber ore vein	Quartz	8	0.07	15.1
	Sphalerite	3	0.12	–
Terezia ore vein	Quartz	3	0.22	14.0
	Sphalerite	3	3.1	38.0
Spitaler ore vein	Quartz	1	0.01	7.2
	Sphalerite	4	2.1	–
	Galena	3	1.5	–
	Barite	1	0.6	–
Rozalia ore vein	Calcite	1	1.5	–

Note: *n* is the number of measurements.

The investigation of primary inclusions in quartz and sanidine from the Vyhne rhyolites revealed high concentrations of N_2 (7.8–9.5 g/kg H_2O) and CO_2 (57–61 g/kg H_2O) in the magmatic fluid. These results are given in Table 8 and were obtained by gas chromatography using the method described by Naumov *et al.* [37]. In addition, the table shows data on the concentrations of volatiles in fluid inclusions in the minerals of the ore veins. These results presented in Table 8 allowed us to draw the following conclusions. (1) The concentration of nitrogen in the rhyolite groundmass is 50 times lower than that during the crystallization of quartz and sanidine phenocrysts. This suggests considerable degassing of the felsic magma during its ascent from great depths (indicated by high pressures in primary fluid inclusions) to the Earth's surface. (2) The higher concentration of nitrogen in the magmatic fluid (8.6 g/kg H_2O) compared with the hydrothermal solutions that formed the ore veins (0.01–3.1 g/kg H_2O, averaging 0.96 g/kg H_2O) is probably also explained by the considerable difference in pressure.

The silicate melt from which the quartz of granodiorites crystallized contained 6.1–4.2 wt % H_2O and was trapped at temperatures of 750–680°C and pressures of 3.8–2.9 kbar. The magmatic fluids were represented by chloride melts (brines) with salt concentrations of 80–77 wt % trapped at temperatures of 640–620°C and pressures of 4.0–3.6 kbar. It is evident that the physicochemical parameters obtained from the inclusions of magmatic melts and fluids recorded the final phase of crystallization of granodiorite melt, and the initial parameters of the melt at the moment of

intrusion must be higher. The postmagmatic fluids trapped in secondary inclusions show a wide range of temperatures from 560 to 225°C, and a temperature decrease is accompanied by a decrease in pressure (from 2.9 to 0.11 kbar) and salt concentration (from 68 to 1.4 wt %). The similarity of the evolution trends of postmagmatic fluids in the intrusive and subvolcanic environments suggests the existence of a single evolutionary trend of hydrothermal systems in the large volume of the ore-forming system.

It is evident that magmatic-stage inclusions in minerals of extrusive rocks recorded earlier conditions compared with magmatic inclusions in quartz from intrusive granodiorites, because extrusive rocks begin to crystallize at higher temperatures than intrusive rocks owing to the release of volatiles. Their magmatic fluid is an aqueous solution with moderate salt concentrations. On the other hand, the magmatic fluid of a later and lower temperature stage of quartz crystallization in granodiorite is a concentrated chloride brine (melt). This is probably related to the accumulation of chlorides in the fluid phase during granodiorite melt crystallization. The evolution of magmatic fluid from diluted aqueous solution to chloride brine (melt) is recorded in variations in the compositions of magmatic fluid inclusions from igneous rocks of various depth levels. Thus, during the crystallization of the intrusive granodiorite body, chlorides accumulated in the fluid phase up to the formation of chloride brine (melt) showing a high density (1.61–1.58 g/cm^3) and a salt concentration of up to 80 wt % and containing ore metals (opaque phases). It is reasonable to suggest that such fluids were derived from the magma chamber.

The postmagmatic stage was accompanied by the mixing of the concentrated chloride brine with diluted solutions. The salt concentration of the magmatic fluid declined with decreasing temperature and pressure. The decrease of these parameters continued until they approached those of fluids responsible for the formation of ore mineralization. The low-concentration solutions that diluted the magmatic fluid could be of meteoric origin. The results of measurements of the hydrogen and oxygen isotopic compositions of micas from the wall-rock metasomatites supported this suggestion. The ores were formed at shallow depths in open fractures, and their precipitation was accompanied by solution boiling, a temperature decrease, and an inflow of meteoric water. The investigation of the compositions of ore-forming fluids showed that they were rich in gold, silver, copper, lead, zinc, and some other elements.

The data reported here suggest that the conditions of ore formation in Banska Stiavnica were similar to those of such typical epithermal ores of the quartz–adularia–sericite type as the Creede, Tonopah, and Colqui deposits [38]. The established evidence for recycling, periodic boiling, and mixing of deep relatively concentrated hot fluids with low-salinity chloride meteoric waters of the surface zone increases the similarity and indicates that the Banska Stiavnica deposits, as well as other similar deposits, is a meteoric–hydrothermal convection system.

ACKNOWLEDGMENTS

The authors thank O.F. Mironova, N.I. Savel'eva, S.A. Gorbacheva, and T.B. Zhukova for carrying out the chemical analyses. This study was financially supported by the Russian Foundation for Basic Research, project nos. 04-05-64407 and 04-05-65123.

REFERENCES

1. R. J. Bodnar, T. J. Reynolds, and C. A. Kuenh, "Fluid Inclusion Systematic in Epithermal Systems," Rev. Econ. Geol. **2**, 73–97 (1985).
2. V. A. Kovalenker, S. Jelen, K. A. Levin, *et al.*, "Mineral Assemblages and Physicochemical Model of the Formation of Gold–Silver–Polymetallic Mineralization of the Deposit Banska Stiavnica (Central Slovakia)," Geol. Carpath. **42**, 291–302 (1991).
3. J. W. Hedenquist and J. B. Lovenstern, "The Role of Magmas in the Formation of Hydrothermal Ore Deposits," Nature **370**, 519–527 (1994).
4. J. W. Hedenquist, "The Ascent of Magmatic Fluid: Discharge Versus Mineralization," in *Magmas, Fluids, and Ore Deposits*, Ed. by J. F. H. Thompson, MAC Short Course Ser. **23**, 263–286 (1995).
5. J. R. Graney and S. E. Kesler, "Gas Composition of Inclusion Fluid in Ore Deposits: Is There a Relation to Magmas?," in *Magmas, Fluids, and Ore Deposits*, Ed. by J. F. H. Thompson, MAC Short Course Ser. **23**, 221–246 (1995).
6. J. R. Richards, "Alkalic-Type Epithermal Gold Deposits: A Review," in *Magmas, Fluids, and Ore Deposits*, Ed. by J. F. H. Thompson, MAC Short Course Ser. **23**, 367–400 (1995).
7. S. F. Simmons, "Magmatic Contributions to Low-Sulfidation Epithermal Deposits," in *Magmas, Fluids, and Ore Deposits*, Ed. by J. F. H. Thompson, MAC Short Course Ser. **23**, 455–478 (1995).
8. W. F. Giggenbach, "The Origin and Evolution of Fluids in Magmatic–Hydrothermal Systems," in *Geochemistry of Hydrothermal Ore Deposits*, Ed. by H. L. Barnes (Wiley, New York, 1997), 3rd ed., pp. 737–796.
9. D. O. Hayba, "Environment of Ore Deposition in the Creede Mining District, San Joan Mountains, Colorado: V. Epithermal Mineralization from Fluid Mixing in the OH Vein," Econ. Geol. **92**, 29–44 (1997).
10. V. A. Kovalenker, V. L. Rusinov, Yu. G. Safonov, *et al.*, "Epithermal Ore-Forming Fluid–Magmatic Systems," in *Abstracts of the International Symposium "General Problems in the Study of Magmatic Ore Deposits"* (IGEM, Moscow, 1997), pp. 39–40 [in Russian].
11. J. Lexa, J. Stol, and V. Konecny, "Banska Stiavnica Ore District: Relationship among Metallogenetic Processes and Geological Evolution of the Central Volcanic Zone," Miner. Deposita **34**, 639–654 (1999).

12. L. Sombathy, "Towards the History of Gold Extraction in Slovakia," Mineral. Slovak. **31**, 401–404 (1999).
13. N. C. White and J. W. Hedenquist, "Epithermal Environments and Styles of Mineralization: Variations and Their Causes, and Guidelines for Exploration," J. Geochem. Explor. **36**, 445–474 (1990).
14. P. Heald, N. K. Foley, and D. O. Hayba, "Comparative Anatomy of Volcanic-Hosted Epithermal Deposits: Acid–Sulfate and Adularia–Sericite Types," Econ. Geol. **82**, 1–26 (1987).
15. V. B. Naumov, V. A. Kovalenker, V. L. Rusinov, and N. N. Kononkova, "Dense Juvenile Water Inclusions in Phenocrysts of Rhyolites," Petrologiya **2**, 480–494 (1994).
16. I. V. Chernyshev, M. Haber, V. A. Kovalenker, *et al.*, "To the Age Position of the Magmatic Events and Epithermal Au–Ag–Base Metal Mineralization in the Central Zone of the Banska Stiavnica Stratovolcano: K–Ar Data," Geol. Carpath. **46**, 327–334 (1995).
17. J. Lexa, "Post-Caldera Epithermal Veins of the Stiavnica Stratovolcano," in *Epithermal Mineralization of the Western Carpathians*, Guidbook Ser. Soc. Econ. Geol. **31**, 249–257 (1999).
18. J. Lexa, P. Kodera, J. Prcuch, *et al.*, "Multiple Stages of Mineralization at the Rozalia Mine, Hodrusha Epithermal Mineralization of the Western Carpathians," in *Epithermal Mineralization of the Western Carpathians*, Guidbook Ser. Soc. Econ. Geol. **31**, 249–257 (1999).
19. V. Konecny, J. Lexa, and V. Hojstricova, "The Central Slovakia Neogene Volcanic Field: A Review," Acta Volcanol. **7** (2), 63–78 (1995).
20. V. B. Naumov, M. L. Tolstykh, V. A. Kovalenker, and N. N. Kononkova, "Fluid Overpressure in Andesite Melts from Central Slovakia: Evidence from Inclusions in Minerals," Petrologiya **4**, 283–294 (1996) [Petrology **4**, 265–276 (1996)].
21. P. Kodera, A. H. Rankin, and J. Lexa, "Evolution of Fluid Responsible for Iron Skarn Mineralization: An Example from the Vyhne–Clococ Deposit, Western Carpathians, Slovakia," Contrib. Mineral. Petrol. **64**, 119–147 (1998).
22. I. Kraus, I. V. Chernyshev, V. Sucha, *et al.*, "Use of Illite for K/Ar Dating of Hydrothermal and Base Metal Mineralization in Central Slovak Neogene Volcanic Rocks," Geol. Carpath. **50**, 353–364 (1999).
23. V. A. Kovalenker, V. Yu. Prokophiev, M. Haber, and S. Jelen, "Banska Stiavnica Epithermal Fluid–Magmatic System: Fluid/Salt Melt Inclusions Studies," Geol. Carpath. **50** (Spec. Issue), 188–189 (1999).
24. V. A. Kovalenker and V. Yu. Prokof'ev, "Epithermal Ore-Forming System of Banska Stiavnica, Central Slovakia: Fluid Regime of Gold–Silver–Base-Metal Mineralization" in *Fluid Flows in the Earth's Crust and Mantle* (IGEM, Moscow, 2002), pp. 91–97 [in Russian].
25. J. Burian, M. Slavkay, J. Stohl, and J. Tozser, in *Metallogeny of Slovak Neovolcanites* (Alfa, Bratislava, 1985), pp. 1–269.
26. I. Mat'o, T. Sasvari, J. Bebej, *et al.*, "Structurally-Controlled Vein-Hosted Mesothermal Gold–Quartz and Epithermal Precious and Base Metal Mineralization in the Banska Hodrusa Ore Field, Central Slovakia Neovolcanites," Mineral. Slov. **28**, 455–490 (1996).
27. V. B. Naumov, "Thermometry of Melt Inclusions in Quartz Phenocrysts of Quartz Porphyries," Geokhimiya, No. 4, 494–498 (1969).
28. V. B. Naumov, "Determination of Volatile Component Concentration and Pressure in Magmas," Geokhimiya, No. 7, 997–1007 (1979).
29. R. J. Bodnar and M. O. Vityk, "Interpretation of Microthermometric Data for H_2O–NaCl Fluid Inclusions," in *Fluid Inclusions in Minerals: Methods and Applications*, Ed. by B. De Vivo and M. Frezzotti (Pontignano-Siena, 1994), pp. 117–130.
30. O. F. Mironova, V. B. Naumov, and A. N. Salazkin, "Nitrogen in Mineral-Forming Fluids: Gas Chromatography of Inclusions in Mineral," Geokhimiya, No. 7, 979–991 (1992).
31. N. I. Savel'eva, V. Yu. Prokof'ev, A. M. Dolgonosov, *et al.*, "Use of Ion Chromatography in Studies of the Anion Composition of Fluid Inclusions," Geokhimiya, No. 3, 401–408 (1988).
32. V. B. Naumov, I. P. Solovova, V. I. Kovalenker, *et al.*, "Juvenile Water under Pressures of 15–17 kbar and Its Concentration in Magma: First Data on Inclusions in Plagioclases of Andesites," Dokl. Akad. Nauk **324**, 654–658 (1992).
33. V. B. Naumov, M. L. Tolstykh, V. A. Kovalenker, and N. N. Kononkova, "Fluid Overpressure in Andesite Melts from Central Slovakia: Evidence from Inclusions in Minerals," Petrologiya **4**, 283–294 (1996) [Petrology **4**, 265–276 (1996)].
34. V. B. Naumov, I. P. Solovova, V. I. Kovalenker, *et al.*, "First Data on Dense Juvenile Water Inclusions in Phenocrysts of Rhyolites," Dokl. Akad. Nauk SSSR **318**, 187–190 (1991).
35. V. B. Naumov, V. I. Kovalenker, V. L. Rusinov, and N. N. Kononkova, "Inclusions of High-Density Magmatic Water in Phenocrysts from Acid Volcanics of the Western Carpathians and Central Tien Shan," Petrologiya **2**, 480–494 (1994) [Petrology **2**, 424–437 (1994)].
36. A. A. Kadik, E. B. Lebedev, and N. I. Khitarov, *Water in Magmatic Melts* (Nauka, Moscow, 1971) [in Russian].
37. V. B. Naumov, O. F. Mironova, A. N. Salazkin, *et al.*, "Magmatic Nitrogen and Its Role in Epithermal Ore Mineralization," Dokl. Akad. Nauk **322**, 973–976 (1992).
38. D. O. Hayba, F. M. Bethke, P. Heald, and N. K. Foley, "Geological, Mineralogical, and Geochemical Characteristics of Volcanic-Hosted Epithermal Precious-Metal Deposits," in *The Geology and Geochemistry of the Epithermal System*, Rev. Econ. Geol. **2**, 129–167 (1985).